SSC18-WKIV-05

Attitude Control optimization of a Virtual Telescope for X-ray observations

Reza Pirayesh, Asal Naseri,
University of New Mexico
Albuquerque, NM, 87131, USA; 5059005809
rpirayeshshirazinezh@unm.edu
Steven Stochaj
New Mexico State University
Las Cruces, NM, 88003, USA
Neerav Shah
NASA Goddard Space Flight Center
Greenbelt, MD, 20771, USA
John Krizmanic
University of Maryland, Baltimore County
Las Cruces, NM, 88003, USA

ABSTRACT

In this paper, a novel approach is investigated for the attitude control of two satellites acting as a virtual telescope. The Virtual Telescope for X-ray Observations (VTXO) is a mission exploiting two 6U-CubeSats operating in precision formation. The goal of the VTXO project is to develop a space-based, X-ray imaging telescope with high angular resolution precision. In this scheme, one CubeSat carries a diffractive lens and the other one carries an imaging device to support a focal length of 100 m. In this mission, the attitude control algorithms are required to keep the two spacecrafts in alignment with the Crab Nebula observations. To meet this goal, the attitude measurements from the gyros and the star trackers are used in an extended Kalman filter, for a robust hybrid controller. Due to limited energy and the requirement of high accuracy, the energy and accuracy of attitude control is optimized for this mission.

NOMENCLATURE

$i, \Omega, \omega, a, e, f$ = inclination, right ascension of the ascending node, argument of Perigee, semi major axis, eccentricity, true anomaly
h = angular momentum about the center of mass
G = gravitational constant
M = mass of the Earth
r = distance between the Earth and satellite
I = moment of Inertia
R^{bo} = rotation matrix
F_i = inertial reference frame
F_o = orbital reference frame
F_b = body reference frame
T = torque
P = proportional gain
D = Derivative gain

INTRODUCTION

Formation flying, a key factor in spacecraft formation and rendezvous, is investigated in many space missions including virtual telescopes. The formation flying role is to keep the spacecraft in an accurate alignment so that they can perform a specific mission. The European Space Agency (ESA) has proposed a mission, Proba3[1,2], that enables pointing towards the sun through a formation in a highly elliptical orbit, and this formation keeps the relative position error in the order of millimeters and the attitude angular error in the order of arc seconds. Another mission at ESA is SIMBOL_X[3], which is a virtual X-ray telescope with 10 arcsecond accuracy. Other virtual telescope missions are X-ray Milli-Arc-Second Structure Imager (MASSIM)[4], and the New Worlds Observer (NWO)[5] exoplanet mission. Calhoun[6] investigated formation flying with noise in the measurements. Woffinden[7] and Okasha[8] investigated the guidance, navigation, and control problem for orbital rendezvous with noise in the measurements and used an extended Kalman filter (EKF) to reduce them. Schacher[9] constructed a robust optimal PID feedback controller considering stochastic uncertainties in the initial conditions. In this optimal

controller, the cost functions are tracking error and regulator cost. Pirayesh, et al.[10-11] investigated the formation control of VTXO.

The Virtual Telescope for X-ray Observations mission, VTXO, uses an innovative design based on diffractive optics with a Phased Fresnel Lens (PFL). The telescope elements (lens and camera) will be separately located on two small satellites, flying in precision formation, to accommodate the required focal length (100 m) of the system. This focal length is required since the PFL requires this length to study the X-Ray resources with high resolutions[12]. In addition, high resolutions of the images require the satellites to be in high angular precision formation for the period they observe the Crab Nebula, i.e., one hour. To meet this goal, 3 main steps in the design are taken based on the desired period and the desired angular precision the satellites should maintain during formation. These steps, each of which are discussed in more detail later, include designing the orbits and the corresponding phases in each of them, the control algorithms, and the filter to reduce the noise of the sensors.

The mission design for the VTXO calls for the two vehicles to hold a rigid formation near apogee, during which time the two spacecraft will perform scientific observations for a short period of time (1h – 3h). While away from apogee the two vehicles will reposition themselves for the next iteration of the observations. Hence, each orbit consists of three major phases: the formation stabilization phase, the development phase, and the scientific phase. The high precision alignment requirements for the mission call for precise knowledge of both spacecraft's position relative to one another. The second aspect of formation flying is attitude determination and control. In the formation stabilization phase, the CubeSats are stabilized while they pass the perigee to come into the next orbit phase, where only an anti-gravity gradient torque is applied to the satellites to lessen the drift of the angular velocities from zero. In the development phase, the coarse pre-attitude control is applied to provide enough attitude accuracy for the scientific phase. In the scientific phase, the precision attitude control takes place, where the two satellites point at the Crab Nebula for one hour.

The attitude control is based on the Quaternion models of the two satellites. In this model, different resources of noises and disturbances including the space (gravity-gradient torques, random accelerations, J2 gravity model, and torques to account for drag, solar pressure, higher-order-gravity terms, etc.), the measurement sensors, and the actuator torques are included[7]. In the attitude control and EKF design, the noises of different sensors including the IMU sensor, and the star tracker are considered, and the navigation part of the control system uses EKF to approximate the angles and the angular velocities of the satellites based on the noisy data from the sensors.

Various initial conditions, due to not clearly known initial conditions and noise in the dynamical system, lead to different errors and energy consumptions assuming the same controller's parameters. This is not desired in the system since energy is limited on the satellite, and besides, the goal of the mission is to obtain the least error. As a result, there are two objective functions to minimize, the energy consumption and the error. To find the optimal parameters of the controllers, a heuristic optimization method, the multi objective genetic algorithm, is used to find the controllers' optimal parameters in the development phase and scientific phase. Since the initial conditions are not known in the development phase, and different ratios of total errors to total energy consumption is desired based on the mission, a neural network is utilized to estimate the optimal controllers' parameters based on the initial quaternion, initial velocity, and different ratios of total errors to total energy consumption.

ORBIT DESIGN

The orbits of the follower and the leader are designed based on the position of the Crab Nebula. The orbits are placed in the same plane and both of their apogees are in the same line connecting the Crab Nebula to the center of the earth so that the satellites have more time to observe the Crab Nebula. The Crab Nebula right ascension and delineation are $5^h\,34^m\,31.94^s$ and 22 degrees, respectively. The orbits have the same right ascension of the ascending node, argument of perigee, and inclination. In addition, the orbits must have the same semi-major axis to have the same period. The only difference between the orbits is their eccentricity. The leader and the follower are both geostationary transfer orbits. The eccentricity of the orbit of the follower is designed to include a 6-minute buffer between the time the follower and the leader pass the point where the orbits intersect each other, to avoid collision between the satellites. The more the difference between the eccentricities are, the lower the risk of collision is, since the satellites would have longer distances between each other. But this results in a higher energy that is needed to keep the desired 100 m relative distance between the satellites. This is because the distance between the apogees of the satellites increases, which requires higher energy to keep the satellites in the relative distance range that is desired. The orbits with respect to the Crab Nebula are shown in the Fig. 1. The orbital elements are given in Table 1.

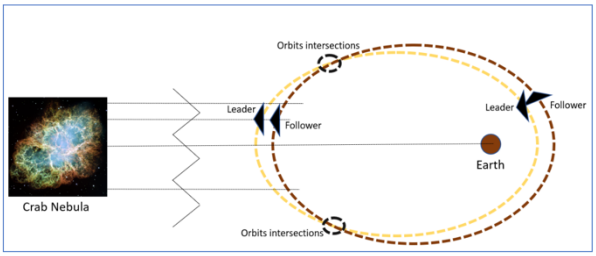

Figure 1: Orbits

Table 1: Orbital elements

	i, rad	Ω, rad	ω, rad	a, km	e
Follower	0.34	0	4.6743	24320	0.7125
Leader	0.34	0	4.6743	24320	0.7336

MODELING THE SATELLITES

To model the system, 4 steps are taken. Since the desired angular velocity and the desired angular acceleration are needed and the values are only known based on the Euler angles, in the first step, the dynamics of the system based on Euler angles is driven. Second, the dynamics of the satellites, considering all the noises in the system based on the quaternions, is driven. Third, the EKF is added to the system of equations to decrease the noise of the sensors and increase the desired resolution. Fourth, a multi objective genetic algorithm and neural network is implemented on the system to optimize energy and errors.

Modelling the satellites with Euler angles

The Earth coordinate frame is the Earth-centered inertia (ECI) frame and the frames used for the satellites are the Local-Vertical-Local-Horizontal (LVLH) frames. The attitude dynamics of the two satellites are driven based on the Euler angles. The rotational equation of motion for the satellites as rigid bodies in space is

$$\boldsymbol{I}\dot{\boldsymbol{\omega}}_b^{\,bi} = -\boldsymbol{\omega}_b^{\,bi} \times \boldsymbol{I}\boldsymbol{\omega}_b^{\,bi} + 3\frac{GM}{r^3}\boldsymbol{o}_3 \times \boldsymbol{J}_b\boldsymbol{o}_3 + \boldsymbol{\tau} \qquad (1)$$

T is the input torques generated by the reaction wheels and random space noises, which are gravity-gradient torques, random accelerations, J2 gravity model, and torques to account for drag, solar pressure, higher-order-gravity terms, etc. In the LVLH frame, the vector $\boldsymbol{o}_3$ is the nadir vector; i.e., $\boldsymbol{o}_3 = -\boldsymbol{r}/r$, which is the third column of the rotational matrix $\boldsymbol{R}^{bo}$. $\boldsymbol{R}^{bo}$ represents the rotational matrix from the frame F_o, which is the orbital frame, to F_b, which is the body fixed frame. $\boldsymbol{o}_1$ is pointing in the direction of the velocity vector, and $\boldsymbol{o}_2$ completes the right-handed triad. If 1-2-3 rotation sequence from F_o to F_b is chosen, then the gravity-gradient torque is

$$\boldsymbol{R}^{bo} = \boldsymbol{R}_3(\theta_3)\boldsymbol{R}_2(\theta_2)\boldsymbol{R}_1(\theta_1)$$
$$\boldsymbol{g}_b = 3\frac{GM}{r^3}\begin{bmatrix} (I_3 - I_2)c_1c_2(s_1c_3 + c_1s_2s_3) \\ (I_3 - I_1)c_1c_2(s_1s_3 + c_1s_2c_3) \\ (I_2 - I_1)(s_1s_3 - c_1s_2c_3)(s_1c_3 + c_1s_2s_3) \end{bmatrix} \qquad (2)$$

The "c" represents cosines of rotations and "s" represents sines of rotations and the index shows the axis of rotation. The $\boldsymbol{\omega}_b^{\,bi}$ is the angular velocity of F_b with respect to F_i. It is obtained from the following equation:

$$\boldsymbol{\omega}_b^{\,bi} = \boldsymbol{\omega}_b^{\,bo} + \boldsymbol{\omega}_b^{\,oi} \qquad (3)$$

If we consider small angles, assuming the orbits to be circular and assuming free motion without any torque on the satellites, the set of the linearized equations that are used in many references are as the following[13]

$$\begin{aligned} &I_1\ddot{\theta}_1 + (I_2 - I_3 - I_1)\omega_c\dot{\theta}_3 - 4(I_3 - I_2)\omega_c^{\,2}\theta_1 = 0 \\ &I_2\ddot{\theta}_2 + 3(I_1 - I_3)\omega_c^{\,2}\theta_2 = 0 \\ &I_3\ddot{\theta}_3 + (I_3 + I_1 - I_2)\omega_c\dot{\theta}_1 + (I_2 - I_1)\omega_c^{\,2}\theta_3 = 0 \\ &\omega_c = \sqrt{\frac{GM}{r^3}} \end{aligned} \qquad (4)$$

As the phrase "linearized equations" suggests, the equations are only valid for small values of Euler angles. Thus, the nonlinear equations are developed

$$\begin{aligned} &\boldsymbol{\omega}_b^{\,oi} = \boldsymbol{R}^{bo}\boldsymbol{\omega}_o^{\,oi} \\ &\boldsymbol{\omega}_o^{\,oi} = \begin{bmatrix} 0 \\ -\dot{f} \\ 0 \end{bmatrix} \\ &\dot{f} = \frac{h}{r^2} \\ &h = \sqrt{p\mu} \\ &p = a(1 - e^2) \\ &\ddot{f} = 2\frac{\mu^2}{h^3}(1 + e\cos(f))(-e\dot{f}\sin(f)) \end{aligned} \qquad (5)$$

Hence, the angular velocity and angular acceleration using Eq. (3) and Eq. (5) are

$$\dot{\boldsymbol{\omega}}_b^{bi} = \boldsymbol{M}\ddot{\theta} + \boldsymbol{G}(\dot{\theta}_1, \dot{\theta}_3, \dot{\theta}_2, \theta_1, \theta_3, \theta_2, \dot{f}) + \ddot{f}\,\boldsymbol{b}(\theta_1, \theta_3, \theta_2)$$

$$\boldsymbol{\omega}_b^{bi} = \begin{bmatrix} c_2c_3\dot{\theta}_1 + s_3\dot{\theta}_2 \\ -c_2s_3\dot{\theta}_1 + c_3\dot{\theta}_2 \\ s_2\dot{\theta}_1 + \dot{\theta}_3 \end{bmatrix} - \dot{f}\begin{bmatrix} s_1s_2c_3 \\ c_1c_3 - s_1s_2s_3 \\ -s_1c_2 \end{bmatrix} \quad (6)$$

$$\boldsymbol{\theta} = \begin{bmatrix} \theta_1 \\ \theta_2 \\ \theta_3 \end{bmatrix}$$

$$\boldsymbol{M} = \begin{bmatrix} c_2c_3 & s_3 & 0 \\ -c_2s_3 & c_3 & 0 \\ s_2 & 0 & 1 \end{bmatrix} \qquad \boldsymbol{b} = \begin{bmatrix} -(s_1s_2c_3 + s_3c_1) \\ (s_1s_2s_3 - c_3c_1) \\ s_1c_2 \end{bmatrix}$$

$$\boldsymbol{G} = \begin{bmatrix} -\dot{\theta}_2\dot{\theta}_1s_2c_3 - \dot{\theta}_3\dot{\theta}_1s_3c_2 + \dot{\theta}_3\dot{\theta}_2c_3 - \dot{f}\dot{\theta}_1c_1s_2c_3 - \dot{f}\dot{\theta}_2c_2s_1c_3 + \dot{f}\dot{\theta}_3s_3s_1s_2 + \dot{f}\dot{\theta}_1s_3s_1 - \dot{f}\dot{\theta}_3c_1c_3 \\ \dot{\theta}_2\dot{\theta}_1s_2s_3 - \dot{\theta}_3\dot{\theta}_1c_2c_3 - \dot{\theta}_2\dot{\theta}_3s_3 + \dot{f}\dot{\theta}_1s_1c_3 + \dot{f}\dot{\theta}_3c_1s_3 + \dot{f}\dot{\theta}_1c_1s_2s_3 + \dot{f}\dot{\theta}_2s_1c_2s_3 + \dot{f}\dot{\theta}_3s_1s_2c_3 \\ \dot{f}\dot{\theta}_1c_1c_2 - \dot{f}\dot{\theta}_2s_1s_2 \end{bmatrix}$$

We substitute $\boldsymbol{\omega}_b^{bi}$ and $\dot{\boldsymbol{\omega}}_b^{bi}$ in Eq. (6) to find the equations of motion. Thus, the final equations are

$$\ddot{\boldsymbol{\theta}} = \boldsymbol{M}^{-1}(-\boldsymbol{G}(\dot{\theta}_1, \dot{\theta}_3, \dot{\theta}_2, \theta_1, \theta_3, \theta_2, \dot{f}) - \ddot{f}\,\boldsymbol{b}(\theta_1, \theta_3, \theta_2) + \boldsymbol{I}^{-1}(-\boldsymbol{\omega}_b^{bi} \times \boldsymbol{I}\boldsymbol{\omega}_b^{bi} + 3\frac{GM}{r^3}\boldsymbol{o}_3 \times \boldsymbol{I}_b\boldsymbol{o}_3 + \boldsymbol{\tau})) \quad (7)$$

$$\ddot{\boldsymbol{\theta}} = \boldsymbol{N}(\dot{\theta}_1, \dot{\theta}_3, \dot{\theta}_2, \theta_1, \theta_3, \theta_2, \dot{f}, \ddot{f}) + \boldsymbol{M}^{-1}\boldsymbol{I}^{-1}(\boldsymbol{\tau})) \quad (8)$$

Since the relative position controller is acting on the leader, the leader is not in its natural orbit and so we do not have the f_L, $\dot{f}_L$, and $\ddot{f}_L$ directly that are used in the Eq. (5) (subscripts "*L*" and "*F*" correspond to the leader and the follower satellites, respectively). However, the distance d between the satellites is known, assuming during the formation control the deviation of the relative distance from 100 m is negligible. Since the line connecting the satellites is parallel to the line connecting the Crab Nebula and the Earth, a triangle can be formed and we can find f_L, $\dot{f}_L$, and $\ddot{f}_L$:

$$f_L = \arcsin(d\sin(f_F)/r_L) + f_F \quad (9)$$

f_L is close to f_F since the r_L is much larger than the distance between the satellites. However, to have more accuracy, the $\arcsin(d\sin(f_F)/r_L)$ is considered in the equations. The $\dot{f}_L$ is

$$\dot{f}_L = \dot{f}_F\left(\frac{d}{r_L}(\sin(f_F) - e_F\cos(f_F)) + 1\right) \sim \dot{f}_F \quad (10)$$

And $\ddot{f}_L \sim \ddot{f}_F$.

In Eq. (7), the matrix **M** is singular at $\theta_2 = pi/2\ rad$. Therefore, Eq. (8) cannot be implemented to analyze and control the satellites, thus, the quaternions are used instead since the quaternions do not have this singularity problem. However, Eq. (6) is used to find the desired angular velocity and the desired angular acceleration which are used later in the controller design.

Modeling the system with quaternions

The quaternion $\boldsymbol{q}^{bI}$ represents the orientation of the body frame with respect to the inertial frame, and this orientation is in the body frame. The transformation matrix $\boldsymbol{R}^{bI}$, which is the transformation from the inertial frame to the body frame, corresponds to this orientation. The attitude dynamics model in terms of quaternions is

$$\dot{\boldsymbol{q}}^{bI} = \frac{1}{2}E(\boldsymbol{q}^{bI})\boldsymbol{\omega}_b^{bI} \quad (11)$$

$$\boldsymbol{q} = \begin{bmatrix} q_1 \\ q_2 \\ q_3 \\ q_4 \end{bmatrix} \quad (12)$$

$$E(\boldsymbol{q}) = \begin{bmatrix} q_4\boldsymbol{I}_{3\times3} + [\boldsymbol{q}_{1:3}\times] \\ -\boldsymbol{q}_{1:3}^{T} \end{bmatrix} \quad (13)$$

$$\dot{\boldsymbol{\omega}}_b^{bI} = J^{-1}(-[\boldsymbol{\omega}_b^{bI}\times]J\boldsymbol{\omega}_b^{bI} + \boldsymbol{\tau})$$

$$\boldsymbol{\tau} = \boldsymbol{\tau}_{in} + \boldsymbol{\tau}_g + \boldsymbol{\tau}_d \quad (14)$$

$$\boldsymbol{\tau}_g = 3\frac{GM}{r^3}\boldsymbol{o}_3 \times \boldsymbol{I}_b\boldsymbol{o}_3$$

The term $\boldsymbol{\tau}_d$ corresponds to disturbances in the space environment including gravity-gradient torques, random accelerations, J2 gravity model, and torques to account for drag, solar pressure, higher-order-gravity terms, etc. It is modeled as uncorrelated white noise with the autocorrelation function as

$$E[\boldsymbol{\tau}_d(t)\boldsymbol{\tau}_d(t')^*] = \sigma_{\ddot{\omega}}\boldsymbol{I}_{3\times3}\delta(t - t') \quad (15)$$

The variance is defined by a trial and error process outlined by Lear[14]. The term $\boldsymbol{\tau}_{in}$ corresponds to the controller input so that the satellites' quaternions reach the desired quaternions.

Sensors

The gyro measures the satellites angular velocity and the star tracker measures the orientations of the satellites. The gyro model is

$$\tilde{\omega} = \partial \boldsymbol{R}(\boldsymbol{\varepsilon}_\omega)[\{\boldsymbol{I}_{3\times3} + diag(\boldsymbol{f}_\omega)\}\boldsymbol{\omega} + \boldsymbol{b}_\omega + \boldsymbol{w}_\omega] \quad (16)$$

The superscript ~ indicates measurement, the $\boldsymbol{\omega}$ is the angular velocity of the satellite, $\boldsymbol{\varepsilon}_\omega$ is the misalignment, $\boldsymbol{f}_\omega$ is scale factor biases, $\boldsymbol{b}_\omega$ is the bias, and $\boldsymbol{w}_\omega$ is white noise. The covariance of the white noise

$$E[\boldsymbol{w}_\omega(t)\,\boldsymbol{w}_\omega(t')] = \boldsymbol{B}\,\delta(t-t')$$
$$\boldsymbol{B} = \sigma_g^2 \boldsymbol{I}_{3\times3} \quad (17)$$

$\boldsymbol{b}_\omega$ is defined as

$$\dot{\boldsymbol{b}}_\omega = -\frac{\boldsymbol{b}_\omega}{\tau_b} + \boldsymbol{w}_b \quad (18)$$

where $\boldsymbol{w}_b$ is white noise with the variance σ_b^2. The star tracker model is[8]

$$\tilde{\boldsymbol{q}}^{sI} = \partial \boldsymbol{q}(\boldsymbol{v}_s^s) \otimes \partial \boldsymbol{q}(\boldsymbol{\varepsilon}_s) \otimes \boldsymbol{q}^{sb} \otimes \boldsymbol{q}^{bI} \quad (19)$$

where $\boldsymbol{v}_s^s$ is sensor white noise with the covariance $\boldsymbol{C}$. $\boldsymbol{\varepsilon}_s$ is the misalignment, defined as

$$\dot{\boldsymbol{\varepsilon}}_s = -\frac{\boldsymbol{\varepsilon}_s^s}{\tau_s} + \boldsymbol{w}_s \quad (20)$$

where the $\boldsymbol{w}_s$ is white noise with the variance σ_s^2. The star tracker model can also be represented in terms of its states as

$$\tilde{\boldsymbol{z}}_s = \boldsymbol{R}^{sb}\boldsymbol{\theta}_b + \boldsymbol{\varepsilon}_s + \boldsymbol{v}_s \quad (21)$$

Here the "b" represents the body frame of the satellites and "s" represents the body frame of the star tracker. The $\boldsymbol{\theta}_b$ is obtained from the following relationship of quaternions

$$\delta \boldsymbol{q}^{bI} = \hat{\boldsymbol{q}}^{bI+} \otimes (\hat{\boldsymbol{q}}^{bI-})^{-1} \quad (22)$$

The superscript "+" represents after the filter estimation, discussed more in the navigation section, and the "-" represents before the estimation. The estimation is represented by $\wedge$ superscript.

For small rotations the following equation holds

$$\partial \boldsymbol{q} \approx \begin{bmatrix} \boldsymbol{\theta}/2 \\ 1 \end{bmatrix} \quad (23)$$

Actuators

the reaction wheel is

$$\dot{\boldsymbol{h}} = -[\boldsymbol{\omega}\times]\boldsymbol{h} - \boldsymbol{\tau}_{in} \quad (24)$$

As a result, $\dot{\boldsymbol{h}}$ is the wheel torque applied to the satellites and $\boldsymbol{\tau}_{in}$ is the input control algorithm. The reaction wheels generate torques for a commanded desired torque as

$$\boldsymbol{\tau}_{in} = \delta \boldsymbol{R}(\boldsymbol{\varepsilon}_\tau)[\{\boldsymbol{I}_{3\times3} + diag(\boldsymbol{f}_\tau)\}\hat{\boldsymbol{\tau}}_{\text{desired}} + \boldsymbol{b}_\tau + \boldsymbol{w}_\tau] \quad (25)$$

Where $\boldsymbol{\varepsilon}_\tau$ is the misalignment, $\boldsymbol{f}_\tau$ is the scale factor bias, $\boldsymbol{b}_\tau$ is bias, $\boldsymbol{w}_\tau$ is white noise, and $\hat{\boldsymbol{\tau}}_{\text{desired}}$ is the desired commanded torque.

GNC design

The goal of the Guidance, Navigation, and Control (GN&C) subsystem is to first define a desired trajectory for the system, in our case, the trajectory is the attitude of the satellites, and then control the system efficiently based on this desired trajectory, given the sensors are noisy. The GNC model leads the system to the desired values.

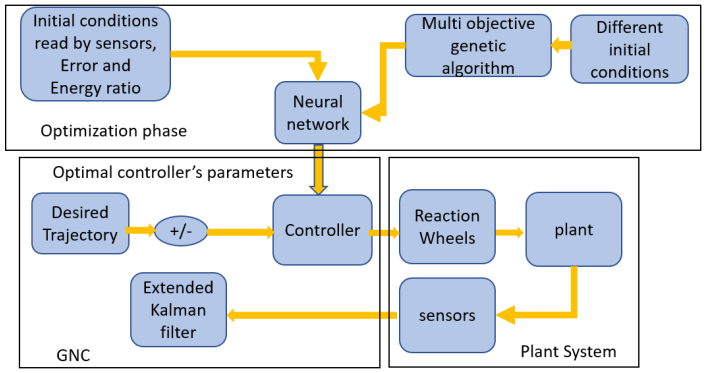

Figure 2: GNC

Guidance

Each satellite is controlled separately so there is no data fusion between the satellites. Each satellite, during the scientific phase, keep their orientation parallel to the line connecting the center of the earth and the Crab Nebula for 1 hour. Accordingly, the desired quaternions for both of the satellites are constant as the following

$$\boldsymbol{q}^{bI} = \begin{bmatrix} -0.5591 \\ 0.0158 \\ -0.0106 \\ 0.8289 \end{bmatrix}$$

And the corresponding Euler angles with 1-2-3 rotation sequence are

$$\begin{bmatrix}\theta_1\\ \theta_2\\ \theta_3\end{bmatrix}=\begin{bmatrix}-2.0235^\circ\\ 0.8173^\circ\\ -68.0144^\circ\end{bmatrix}$$

Navigation

The navigation model uses an extended Kalman filter to estimate the states optimally. The dynamics model used for propagating the states are

$$\hat{\dot{\boldsymbol{q}}}^{bI}=\frac{1}{2}E(\boldsymbol{q}^{bI})(\tilde{\boldsymbol{\omega}}_b{}^{bI}-\hat{\boldsymbol{b}}_\omega) \quad (27)$$

$$\hat{\dot{\boldsymbol{b}}}_\omega=-\frac{\hat{\boldsymbol{b}}_\omega}{\tau_b} \quad (28)$$

$$\hat{\dot{\boldsymbol{\varepsilon}}}_s=-\frac{\hat{\boldsymbol{\varepsilon}}_s^s}{\tau_s} \quad (29)$$

The model for this filter is

$\dot{\boldsymbol{x}}=f(\boldsymbol{x},\boldsymbol{\tau}_{in},\boldsymbol{w},t),\ \boldsymbol{w}\sim N(0,\boldsymbol{B})$

$\boldsymbol{y}_k=\boldsymbol{h}(\boldsymbol{x})+\boldsymbol{v}_k,\ \boldsymbol{v}_k\sim N(0,\boldsymbol{C})$

Initialize: $\boldsymbol{x}_0,\boldsymbol{P}_0$

Propagation:

States $\quad \hat{\dot{\boldsymbol{x}}}=f(\hat{\boldsymbol{x}},\boldsymbol{\tau}_{in},t)$ (30)

Covariance $\quad \hat{\boldsymbol{p}}_k^-=\hat{\boldsymbol{\varphi}}\hat{\boldsymbol{p}}_{k-1}^+\hat{\boldsymbol{\varphi}}^T+\hat{\boldsymbol{Q}}$

Gain $\quad \hat{\boldsymbol{K}}_k=\hat{\boldsymbol{p}}_k^-\hat{\boldsymbol{H}}_k^T[\hat{\boldsymbol{H}}_k\hat{\boldsymbol{p}}_k^-\hat{\boldsymbol{H}}_k^T+\hat{\boldsymbol{R}}]^{-1}$

Update $\quad \hat{\boldsymbol{x}}_k^+=\hat{\boldsymbol{x}}_k^-+\hat{\boldsymbol{K}}_k[\boldsymbol{y}_k-\boldsymbol{h}(\hat{\boldsymbol{x}}_k^-)]$

$\quad\quad \hat{\boldsymbol{p}}_k^+=[\boldsymbol{I}-\hat{\boldsymbol{k}}_k\hat{\boldsymbol{H}}_k]\hat{\boldsymbol{p}}_k^-$

The navigation states of each satellite for the filter comprise a 9-state vector

$$\hat{\boldsymbol{x}}=[\boldsymbol{\theta}_b\ \ \boldsymbol{b}_\omega\ \ \boldsymbol{\varepsilon}_s]_9 \quad (31)$$

The model does not have angular velocities, since the attitude model used in the filter is in the model-replacement mode[15]. The measurements violate the normalization constraint of the quaternions, so a multiplicative error is used to overcome this problem. As a result, instead of 4 elements of quaternions, 3 components of orientation $\boldsymbol{\theta}_b$ are selected for the states[16]. The quaternions are updated with the following equation

$$\hat{\boldsymbol{q}}^{bI+}=\delta\boldsymbol{q}^{bI}(\boldsymbol{\theta}_b)\otimes\hat{\boldsymbol{q}}^{bI-} \quad (32)$$

The sate transition matrix $\hat{\boldsymbol{\varphi}}$ used in the filter is $e^{\boldsymbol{F}\Delta t}$, and it can be approximated by the fourth order Taylor series

$$\boldsymbol{\varphi}=e^{\boldsymbol{F}\Delta t}\approx I+\boldsymbol{F}\Delta t+\frac{\boldsymbol{F}^2\Delta t^2}{2!}+\frac{\boldsymbol{F}^3\Delta t^3}{3!}+\frac{\boldsymbol{F}^4\Delta t^4}{4!} \quad (33)$$

where $\boldsymbol{F}=\frac{\delta \boldsymbol{f}}{\delta \boldsymbol{x}}|_{\boldsymbol{x}_k^-}$. The discrete process noise matrix is

$$\hat{\boldsymbol{Q}}=\begin{bmatrix}\boldsymbol{Q}_g & 0\\ 0 & \boldsymbol{Q}_n\end{bmatrix}_{9\times9} \quad (34)$$

The gyro process noise matrix Q_g is approximated considering the gyro noise is internal and random walk

$$\boldsymbol{Q}_g=\begin{bmatrix}\sigma_{x\,g}^2\Delta t & 0 & 0\\ 0 & \sigma_{y\,g}^2\Delta t & 0\\ 0 & 0 & \sigma_{z\,g}^2\Delta t\end{bmatrix} \quad (35)$$

Q_n represents the biases process noise defined as

$$\boldsymbol{Q}_n=\begin{bmatrix}\sigma_b^2\boldsymbol{I}_{3\times3}(1-e^{-\frac{2\Delta t}{\tau_b}}) & 0_{3\times3}\\ 0_{3\times3} & \sigma_s^2\boldsymbol{I}_{3\times3}(1-e^{-\frac{2\Delta t}{\tau_b}})\end{bmatrix}_{6\times6} \quad (36)$$

The measurement sensitivity matrix $\hat{\boldsymbol{H}}_k$ is

$$\hat{\boldsymbol{H}}_k=\frac{\delta \boldsymbol{h}(\boldsymbol{x})}{\delta \boldsymbol{x}}|_{\hat{\boldsymbol{x}}_k^-}=[R_{3\times3}(\hat{q}^{sb})\quad 0_{3\times3}\quad I_{3\times3}]_{3\times9} \quad (37)$$

Control

For the development phase and scientific phase, 2 controllers are employed for controlling the attitude, a proportional-derivative (PD) controller and a robust sliding mode controller. In the dynamical model, it is assumed that there is a disturbance in the inertial momentum

J = J + disturbance

$$\text{disturbance} = 0.2J^2\begin{bmatrix}\cos(t)\\ \sin(t)\\ 0.5\end{bmatrix} \quad (38)$$

The PD controller is

$$\hat{\boldsymbol{\tau}}_{desired}=P(\boldsymbol{\theta}_{desired})+D(\hat{\boldsymbol{\omega}}_{desired}^{bI}-\hat{\boldsymbol{\omega}}^{bI}) \quad (39)$$

where the desired angular offset is obtained from the small difference orientation feature of quaternions

$$\begin{bmatrix}\boldsymbol{\theta}_{\text{desired}}\\ 1\end{bmatrix}=\hat{\boldsymbol{q}}_{\text{desired}}\otimes(\hat{\boldsymbol{q}}^{bI})^{-1} \quad (40)$$

To define the sliding mode controller (SMC), first the difference in quaternions is defined as

$$\delta\boldsymbol{q}=\begin{bmatrix}\delta\boldsymbol{q}_{1:3}\\ \delta q_4\end{bmatrix} \quad (41)$$

Then the sliding mode vector is defined as

$$\hat{\boldsymbol{s}}=(\hat{\boldsymbol{\omega}}^{bI}-\hat{\boldsymbol{\omega}}_{desired}^{bI})+k\times sign(\delta\hat{q}_4)\delta\hat{\boldsymbol{q}}_{1:3} \quad (42)$$

And finally, the SMC controller is

$$\hat{\boldsymbol{\tau}}_{in} = \boldsymbol{J}\{\frac{k}{2}[|\delta\hat{q}_4|(\hat{\boldsymbol{\omega}}^{bI} - \hat{\boldsymbol{\omega}}^{bI}_{desired}) - sign(\delta\hat{q}_4)\delta\hat{\boldsymbol{q}}_{1:3}(\hat{\boldsymbol{\omega}}^{bI} + \hat{\boldsymbol{\omega}}^{bI}_{desired})] + \hat{\dot{\boldsymbol{\omega}}}^{bI}_{desired} - \boldsymbol{A}\,\bar{\boldsymbol{s}}\} + [\hat{\boldsymbol{\omega}}^{bI}\times]\boldsymbol{J}\hat{\boldsymbol{\omega}}^{bI} \quad (43)$$

where $\boldsymbol{A}$ is a positive definite matrix and $\bar{\boldsymbol{s}}$ is defined with a saturation function as

$$\bar{s}_i = sat(s_i, \varepsilon_i)\ i = 1,2,3 \quad (44)$$

s_i is the i^{th} element of the sliding mode vector, and ε_i is a small positive number.

For the phase 3, to reduce the drift of the angular velocities from zero, the gravity gradient torque is eliminated by an anti-gravity torque applied to the satellites

$$\hat{\boldsymbol{\tau}}_{in} = -\hat{\boldsymbol{\tau}}_g \quad (45)$$

To find the optimal controllers' parameters, two algorithms, multi objective genetic algorithm and neural networks, are utilized. The multi objective genetic algorithm finds the minimum of the defined objective functions by heuristically finding the optimum variables or parameters affecting the objective functions. The objective functions are the error of the controllers and the total energy consumed during the control. The result of this optimization is an optimum pareto front, representing a set of points showing how each objective value changes against the other one.

The neural network creates a function which estimates the optimal controllers' parameters based on the input to the neural network. The outputs and the inputs are different for the development phase and scientific phase.

In the development phase, the objective function of the optimization algorithm is first the total energy consumed during the attitude control and second the error of the last 30 seconds of the control. The parameters to be defined during the optimization are the PD controller's parameters, the SMC's parameters, and the time of the control. The total error of the last seconds, here defined to be 30, is the important duration, since it defines that in the development phase a low error is obtained and so the scientific phase with low errors can be started. This low error helps keep low errors during the scientific phase. The pareto front results of this optimization for one specified initial quaternion and angular velocity for the PD controller and SMC are shown below.

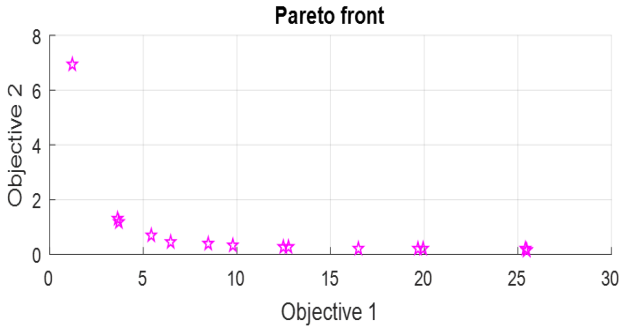

Figure 3: Pareto front

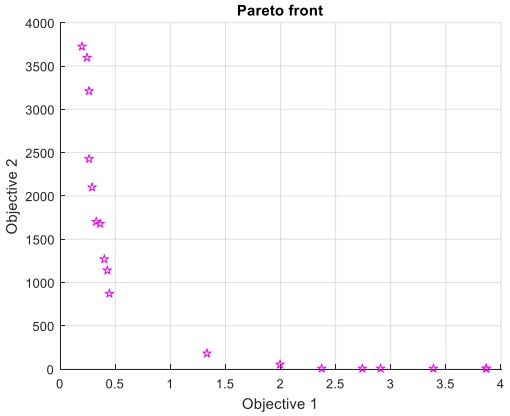

Figure 4: Pareto front

As it is illustrated, when the objective 2, or the total energy consumption, increases, the objective 1, or the total error in the last 30s, decreases and vice versa. This is due to the fact that when there is more energy consumed, the error decreases. This optimization is run for many times for different initial quaternions and angular velocities.

Next, in the neural network step, these quaternions are transformed into Euler angles by 3-2-1 sequence to decrease the number of inputs in the neural network. The inputs to the neural network are then the corresponding Euler angles of the quaternions, the angular velocities, and the ratio of the optimum error value to the total energy consumption. The ratio of the error value to the total energy consumption is obtained from the optimum output of the optimization algorithm. The outputs of the neural network are then the optimal controllers' parameters and time for the development phase. The neural network is designed with 2 hidden layers, which has 10 neurons in the first layer and 3 neurons in the last layer, and 6 inputs and 3 outputs when using PD controller and 4 outputs when using SMC. The number of epochs is set to 1000 and the number of maximum fail is set to be 6000. The

regression and performance plots for the PD controller and SMC are

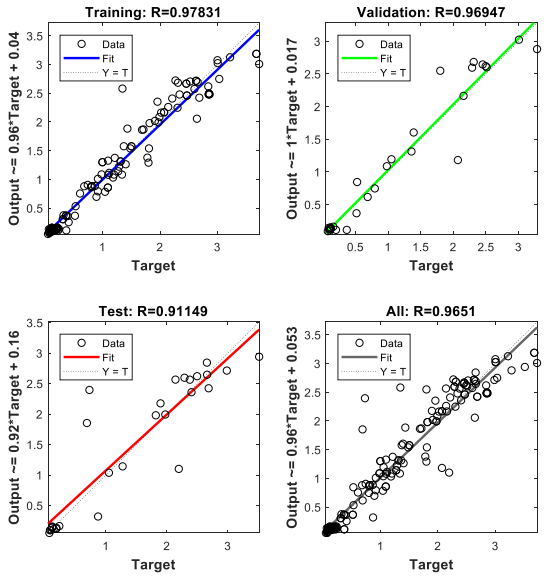

Figure 5: Regression PD controller

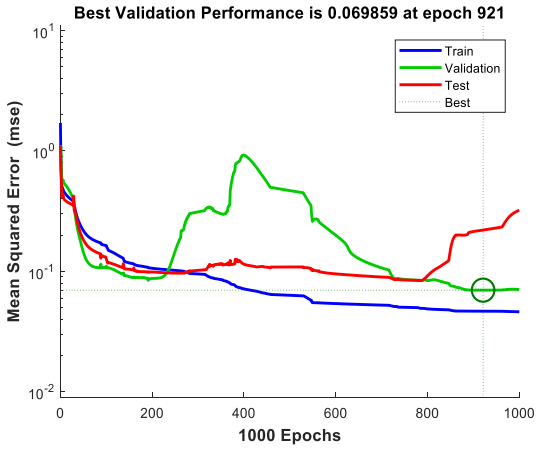

Figure 6: Performance PD controller

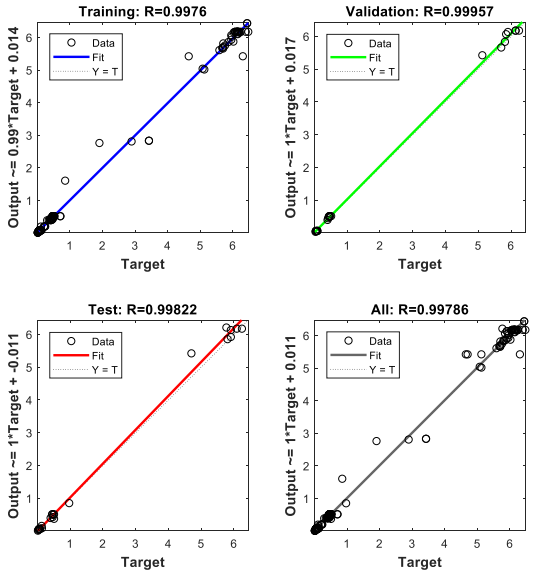

Figure 7: Regression SMC

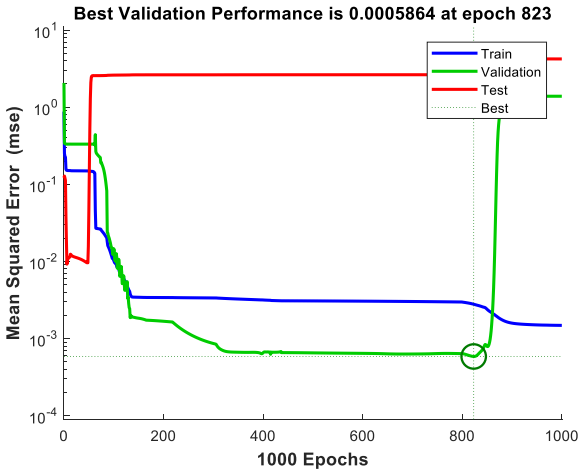

Figure 8: Performance SMC

The performance and regression show the high accuracy of the neural network estimation for the controllers' parameters and time of the development. Table 2 and Table 3 show the estimated controllers' parameters and the development phase duration by the neural network for the PD controller and SMC.

Table 2: Input to the Neural network

Initial quaternion	Initial angular velocity	Ratio of Error to energy
[-0.4028 0.0776 -0.8484 0.3594]	[-0.0353 -0.0788 0.8009]	1.86

Table 3: Output of the Neural network

PD Controller's parameters	SMC's parameters	duration PD, SMC
$\begin{bmatrix} k_p \\ k_d \end{bmatrix} = \begin{bmatrix} 0.2271 \\ 0.3191 \end{bmatrix}$	$\begin{bmatrix} k \\ G \\ eps \end{bmatrix} = \begin{bmatrix} 6.4724 \\ 0.0326 \\ 0.3662 \end{bmatrix}$	0.0649, 0.0543

In the scientific phase, since the initial conditions are so close to each other, only for one initial quaternion and angular velocity the objective functions are optimized. Besides, the time of scientific phase is fixed to be an hour. The Pareto front of the PD controller and SMC are

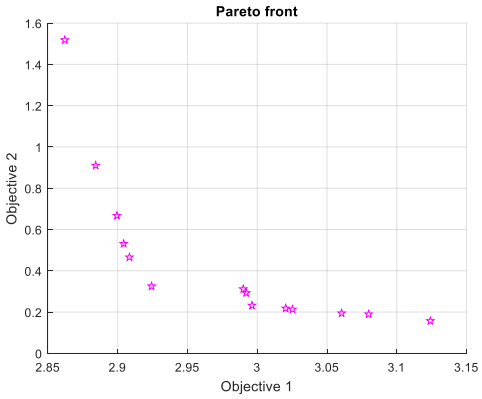

Figure 9: Pareto front

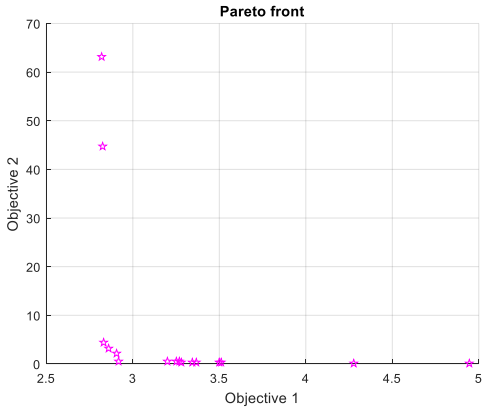

Figure 10: Pareto front

Only the ratio of the error to energy consumption is given to the neural network to estimate the controllers' parameters. These numbers are the output of the optimization algorithm. The performance of the neural network for the PD controller and SMC are

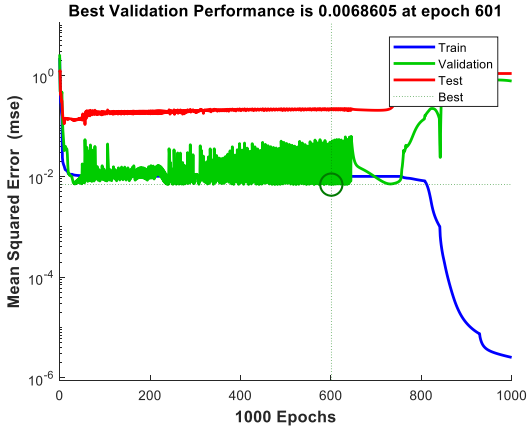

Figure 11: PD controller's performance

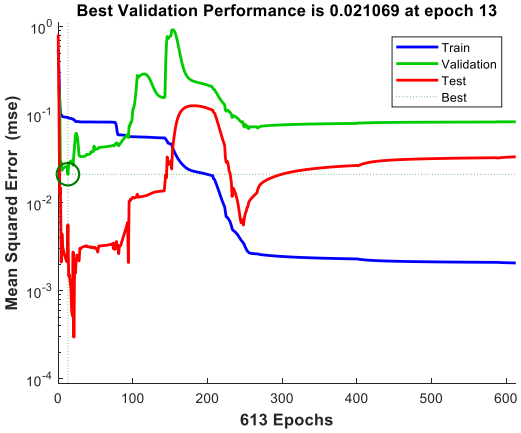

Figure 12: Performance of SMC

The high performance of the neural networks shows the high accuracy of the neural network estimators.

Table 4- Output of the Neural network

Ratio	PD Controller's parameters	SMC's parameters
0.1	$\begin{bmatrix} k_p \\ k_d \end{bmatrix} = \begin{bmatrix} 2.2781 \\ 0.6301 \end{bmatrix}$	$\begin{bmatrix} k \\ G \\ eps \end{bmatrix} = \begin{bmatrix} 2.8800 \\ 0.0050 \\ 0.8866 \end{bmatrix}$

RESULTS

In the development phase, all the subsystems, except camera, are on to provide enough attitude accuracy for the next phase. In the scientific phase, all the subsystems are on and the camera is imaging the Crab Nebula X-ray emissions. In the next phase, the controller switches to the anti-gravity gradient torque to reduce the drift of the satellites angular velocities from zero. Besides, the sensors, the camera, and the EKF are off since this is passive control. Table 2 summarizes the phases. The results of the follower and the leader are the same.

Table 5: Phases

	Controller	Sensors and filters	Camera
Phase1	SMC/PD	On	Off
Phase2	SMC/PD	On	On
Phase3	Anti-gravity gradient torque	Off	off

Phase 1

In this phase, only the camera is off, and the controller and the filters are working. The SMC and PD controller responses are robust as the following

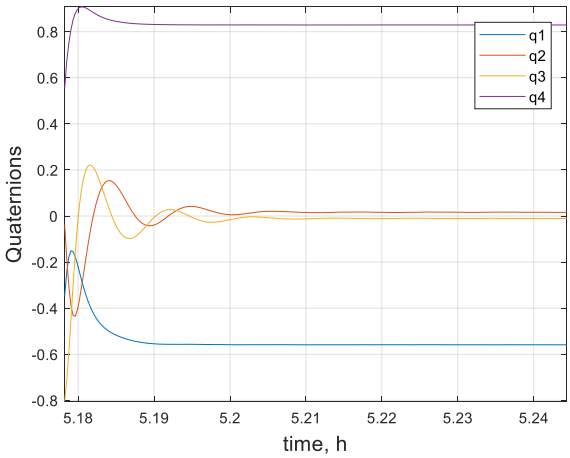

Figure 13: Follower PD

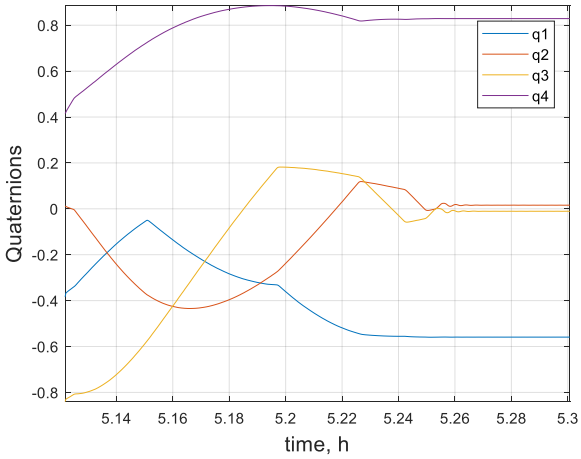

Figure 14: SMC

Phase 2

In this phase, the camera is on and the satellites observe the Crab Nebula for 1 hour. The PD controller and SMC provide the following robust responses

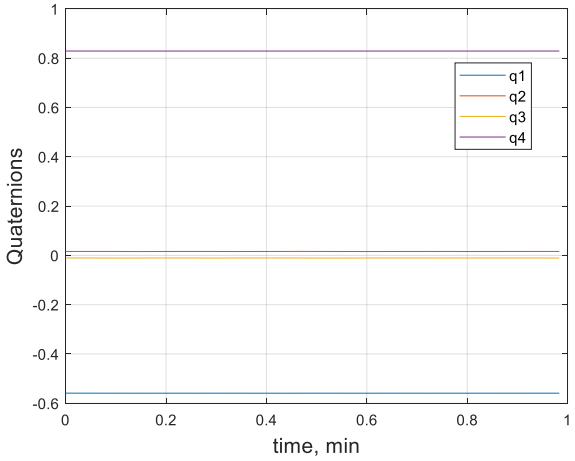

Figure 15: Follower PD controller

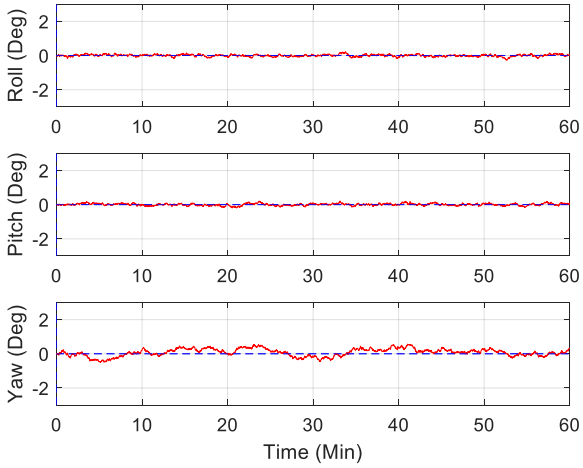

Figure 16: Follower Euler angle error (PD)

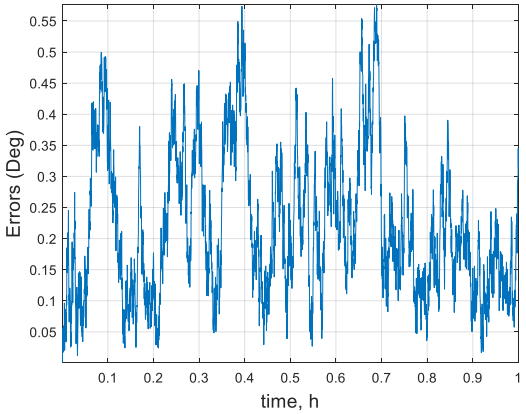

Figure 17- Error (PD)

The average accumulated error in time for the PD controller is 0.2219 deg.

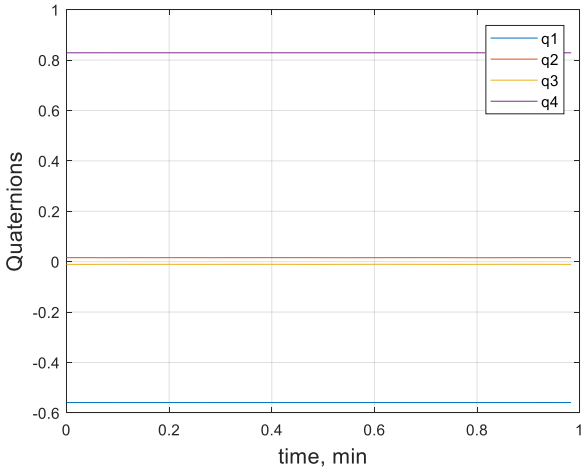

Figure 18: Follower SMC controller

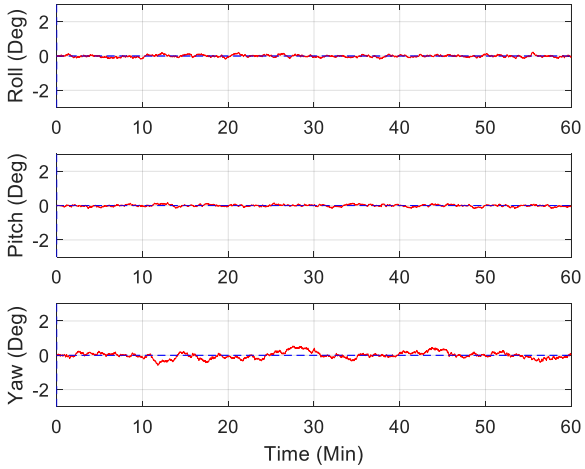

Figure 19: Follower Euler angle error (SMC)

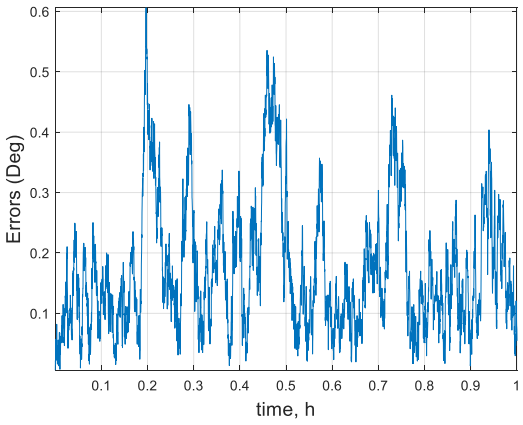

Figure 20-Error (SMC)

The average accumulated error in time for the SMC controller is 0.1738 deg.

These results, considering the disturbances in the inertial momentum, show the robustness of the PD controller. However, PD controllers are not guaranteed to be robust against high disturbances, unlike SMCs. This robustness in SMC is provided at the price of chattering in the controller output fed into the actuators, which are the reaction wheels.

Phase3

In this phase, the anti-gravity gradient torque is applied to decrease the drift of the angular velocity from zero. However, the third angular velocity increases while the other two angular velocities fluctuate around zero.

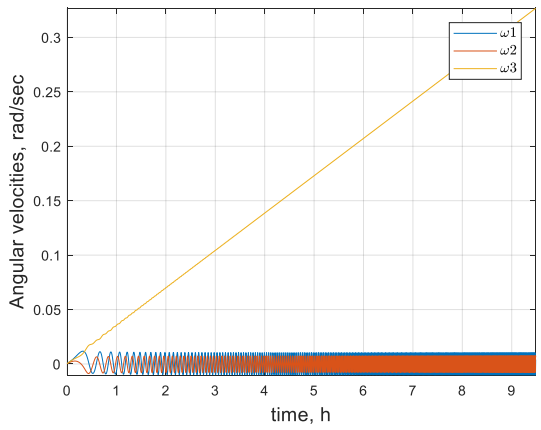

CONCLUSION

VTXO demonstrates the key technologies that should be developed to keep spacecraft in formation. The high accuracy involved in this mission requires more challenging technologies to be developed further such as more advanced controlling algorithms, more accurate filters, and better sensors. The technology that was developed here provides high accuracy with the involved noises influencing the attitude and so the attitude accuracy. To optimize the energy consumption and error, a multi objective genetic algorithm is implemented on the GNC. In the future work, the relative position between the satellites will not be assumed constant and this distance as well will be put into consideration for higher accuracies, since this distance also must be controlled for providing the 100m required distance between the satellites. In addition, the time of different phases will be tuned based on the low energy consumption and high performance of the satellites. Furthermore, the angular velocity in the direction of the Crab Nebula will be tuned and optimized, and the orbits will be designed optimally to optimize the energy and error.

References

1. Sánchez-Maestro, R., Agenjo-Díaz, A., Cropp, A., "PROBA-3 Formation Flying High Performance Control''. 5th International Conference on Spacecraft Formation Flying Missions and Technologies (SFFMT 2013), Munich, Germany, May 29-31, 2013.
2. Peyrard, J., Olmos, D. E., Agenjo, A., Kron, A., Cropp, A.,'' Design and Prototyping of PROBA-3 formation flying system'', International Journal of Space and Engineering, 2014
3. Clédassou, R. and Ferrando, P.,''A new generation hard X-ray formation flying mission'', Journal of Experimental Astronomy, Vol. 20, PP 421-434. Dec 2005
4. G. K. Skinner, Z. Arzoumanian, W. C. Cash et al.," The milliarc-second structure imager (MASSIM): a new concept for a high angular resolution X-ray telescope,"in *Space Telescopes and Instrumentation 2008: Ultraviolet to Gamma Ray*, vol. 7011 of *Proceedings of SPIE*, Marseille, France,June2008.
5. Cash, W., Oakley, P., Turnbull, M., Glassman, T., Lo, A., Polidan, R., Kilston, S., Noecker, C., "The New Worlds Observer: scientific and technical advantages of external occulters", SPIE, 7010, 1Q, 2008.
6. Calhoun, P.C., and Shah, N.,'' Covariance Analysis of Astrometric Alignment Estimation Architectures for Precision Dual Spacecraft Formation Flying'', AIAA Guidance, Navigation, and control Conference 13-16 August 2012, Minneapolis, Minnesota
7. Woffinden, D., Geller, D.,'' Relative Angles-Only Navigation and Pose Estimation for Autonomous Orbital Rendezvous'', Journal of Guidance, control, And Dynamics, Vol. 30, No. 5, September–October 2007
8. Okasha, M. and Newman, B.,'' Relative Motion Guidance, Navigation and Control for Autonomous Orbital Rendezvous'', AIAA Guidance, Navigation, and Control Conference 08 - 11 August 2011, Portland, Oregon
9. Schacher, M. (2009)., "Optimal PID control in case of random initial conditions" PAMM 9, no. 1 (2009): 573-574.
10. Pirayesh, Reza, Asal Naseri, Steven Stochaj, Neerav Shah, and John Krizmanic. "Attitude Control of a Two-CubeSat Virtual Telescope in Highly Elliptical Orbits." In 2018 AIAA Guidance, Navigation, and Control Conference, p. 0866. 2018.

11. Naseri, Asal, Reza Pirayesh, Richard K. Adcock, Steven J. Stochaj, Neerav Shah, and John Krizmanic. "Formation Flying of a Two-CubeSat Virtual Telescope in a Highly Elliptical Orbit." In 2018 SpaceOps Conference, p. 2633. 2018.

12. Kyle, R., Stochaj, S., Shah, N., Krizmanic, J., and Naseri, A.,''VTXO – VIRTUAL TELESCOPE FOR X-RAY OBSERVATIONS'', 9th International Workshop on Satellite Constellations and Formation Flying, June 19-21, 2017, University of Colorado Boulder.

13. Hall, D.C., Spacecraft Attitude Dynamics and Control, April 4, 2011

14. Lear, W. M., Kalman Filtering Techniques, NASA Johnson Space Center: Mission Planning and Analysis Division, Houston, TX, Sept. 1985, JSC-20688.

15. Crassidis, J. L. and Junkins, J. L., Optimal Estimation of Dynamic System, 1st ed., CRC Press LLC, U. S., 2004

16. Pittelkau, M. E., "Rotation Vector in Attitude Estimation," Journal of Guidance, Control, and Dynamics, Vol. 26, No. 6, Nov.–Dec. 2003, pp. 855–859